



30 **1. Introduction**

31 Volatile organic compounds (VOCs) are an important class of organic pollutants in the urban
32 air and have aroused great attention (Kamal et al., 2016; Koppmann, 2008; Mozaffar and Zhang,
33 2020). As one of the typical toxic VOC species, benzene poses a variety of negative impacts on
34 human health including respiratory irritation, asthma, and allergies (Cui et al., 2019; Kim et al.,
35 2013; Tang et al., 2007). Moreover, benzene has high chemical reactivity, and could participate in
36 photochemical reactions in the atmosphere, thereby leading to the formation of secondary organic
37 aerosols (SOA) and ozone (Dumanoglu et al., 2014; Hsu et al., 2018; Li et al., 2019). Given the high
38 toxicity to human health and tremendous harm to air quality (Dumanoglu et al., 2014; Lu et al.,
39 2020), it is highly imperative to decrease the ambient benzene concentration. It was well
40 documented that ambient benzene mainly originated from anthropogenic emission (Mozaffar and
41 Zhang, 2020; Pakkattil et al., 2021). Therefore, understanding the response of ambient benzene to
42 anthropogenic emission was favorable to evaluate the effectiveness of abatement strategies and
43 inform policy decisions.

44 Recently, the ongoing global outbreak COVID-19 has resulted in paroxysmal public health
45 responses including travel restrictions, lockdown, curfews, and quarantines around the world. These
46 drastic lockdown measures inevitably triggered sweeping disruptions of social and economic
47 activities, and further affected the emissions and concentrations of some air pollutants (Bauwens et
48 al., 2020; Berg et al., 2021; Doumbia et al., 2021; Zheng et al., 2021b). The unexpected public health
49 emergency provided us an unprecedented chance to assess the response of air pollutants to emission
50 reduction. Bauwens et al. (2020) has observed that the average NO₂ column in China during
51 January-April 2020 decreased by about 40% relative to the same period in 2019 due to the dramatic
52 decreases of NO_x emissions. Later on, Keller et al. (2021) has analyzed the impact of COVID-19
53 lockdown on global NO₂ concentrations and found that the surface NO₂ concentrations were 18%
54 lower than business as usual from February 2020 onward. In addition, Hammer et al. (2021)
55 estimated that population-weighted mean PM_{2.5} concentrations in China, Europe, and North
56 America experienced changes of -11 to -15, -2 to 1, and -2 to 1 µg/m³ during COVID-19 lockdown
57 period, respectively. To date, most of the current studies focused on regional or global PM_{2.5}, NO₂,
58 and O₃ concentration changes after the COVID-19 outbreak, while few studies assessed the impact



59 of COVID-19 lockdown on ambient benzene levels.

60 Currently, only several studies assessed the impact of COVID-19 lockdown on atmospheric
61 benzene level. Mor et al. (2021) observed that the atmospheric benzene level in Chandigarh, India
62 decreased by 27% during COVID-19 period. Afterwards, Pakkattil et al. (2021) demonstrated that
63 the ambient benzene levels in Delhi (-93%) and Mumbai (-72%) have suffered from drastic
64 decreases after COVID-19 lockdown. Although the ground-level measurement could reflect the
65 regional ambient benzene changes during COVID-19 lockdown period to some extents, few regions,
66 especially in developing countries, have collected sufficient observations for ambient benzene
67 exposure assessment (Geddes et al., 2016; Van Donkelaar et al., 2015). Moreover, the limited
68 monitoring sites around the world cannot accurately reflect the global benzene pollution because of
69 large spatial gaps and restricted spatial representativeness of these ground-based sites (Shi et al.,
70 2018). The health effect assessment based on these scarce sites alone inevitably increased the
71 probability of exposure misclassification (Ling and Li, 2021). Fortunately, chemical transport
72 models (CTMs) gave us an unparalleled chance to capture the full-coverage ambient benzene level
73 at the global scale. Although CTMs generally showed various biases owing to high uncertainties in
74 initial conditions, input variables, and parameterizations (Ivatt and Evans, 2020), the machine-
75 learning bias-correction method could significantly reduce bias in air quality models (Bocquet et al.,
76 2015). Up to date, no study employed the ensemble technique to analyze the change of global
77 ambient benzene after COVID-19 outbreak. Besides, nearly all of the current studies only used
78 original observation data to assess the impact of COVID-19 lockdown on ambient benzene level
79 (Pakkattil et al., 2021). Actually, the concentrations of air pollutants were not only controlled by
80 emission, but also modulated by complex meteorological conditions (Hammer et al., 2021). For
81 instance, some pioneering studies have revealed that several severe haze episodes still occurred even
82 with the strict restrictions put in place in China (Chang et al., 2020; Huang et al., 2021). Hence, it
83 is necessary to remove the effects of meteorological parameters and then to further quantify the
84 isolated contribution of emission reduction to global ambient benzene level and health risks during
85 COVID-19 lockdown period.

86 In our study, the machine-learning model coupled with CTMs was applied to estimate the
87 global ambient benzene concentrations from 23 January to 30 June in 2019 and 2020. At first, the



88 CTMs output, emission inventory, meteorological parameters, and many other geographical
89 covariates were integrated into the ensemble decision tree model to obtain global full-coverage
90 benzene concentrations in the atmosphere. Then, we also examined the synergetic impacts from the
91 anthropogenic emissions and meteorological factors during the pre-lockdown and lockdown periods.
92 Finally, we estimated the emission-induced benzene concentrations before and after COVID-19
93 lockdown and quantified the benzene-related health benefits due to COVID-19 lockdown in major
94 regions around the world. This study shows important implications for developing control strategies
95 to alleviate global atmospheric benzene pollution.

96 **2. Data and methods**

97 2.1 Data preparation

98 2.1.1 Ground-level benzene observation

99 Our analysis was performed based on the recent development of unprecedented public access to
100 ground-level air quality observations. In our study, we collected an air quality dataset of hourly
101 surface benzene observations at 669 sites at the global scale during 23 January-30 June in 2019 and
102 2020 (Figure S1). The detailed spatial distribution of these sites in India, Europe, and the United
103 States are depicted in Figure S1. The surface benzene dataset in India was downloaded from the
104 Central Pollution Control Board (CPCB) online database, which has been widely utilized in
105 previous studies (Mahato et al., 2020; Mor et al., 2021; Sharma et al., 2020). The ground-level
106 benzene observations in Europe and the United States were compiled from air quality data portal of
107 the European Environment Agency (EEA) and United States Environmental Protection Agency
108 (EPA), respectively. All of the database provided data quality assurance (QA) and quality control
109 (QC) programs by establishing strict procedures for sampling, analysis, and calibration (Gurjar et
110 al., 2016). Only days with more than 12 h of available data are included in the analysis. All of the
111 hourly data was average to the daily scale.

112 2.1.2 Independent variables

113 The daily benzene concentrations at global scale were simulated using GEOS-Chem model
114 (v12-01), which included the full gaseous HO_x-O_x-NO_x-CO-NMVOC chemistry and online aerosol
115 calculations. The simulation used assimilated meteorological observations (GEOS MERRA-2) at 2°
116 x 2.5° horizontal resolution with 72 vertical levels for the year 2019 and 2020. The anthropogenic



117 emission inventory in 2019 was collected from Community Emissions Data System (CEDS). Then,
118 the emission inventory in 2020 was calculated based on that in 2019 and updated adjustment factor
119 proposed by Doumbia et al. (2021).

120 The meteorological parameters were obtained from the NASA Goddard Earth Observing
121 System Composition Forecast (GEOS-CF) model (Keller et al., 2021b). GEOS-CF integrates the
122 GEOS-Chem atmospheric chemistry model into the GEOS Earth System Model (Hu et al., 2018;
123 Long et al., 2015) and provides global hourly analyses of meteorological variables at 0.25° spatial
124 resolution (Keller et al., 2021b). Meteorological parameters including surface pressure (PS), relative
125 humidity (RH), 2-m air temperature (T2M), total precipitation (TPREC), 10-m latitudinal wind
126 component (U10M), 10-m longitudinal wind component (V10M), and boundary layer height (BLH)
127 obtained from GEOS-CF were used to develop the model (Figure S2). In addition, cropland, forest,
128 grassland, shrubland, and barren land also have been integrated into the final model (Liu et al., 2020).

129 All of the independent variables collected from multiple sources were regridded to 0.25° grids
130 using spatial interpolation algorithms. During the process of model development, the most important
131 procedure was to remove some redundant explanatory variables and then to determine the optimal
132 variable group. The basic principle of the variable selection was to eliminate the less important
133 predictors. These variables generally suggested that the R^2 value of the submodel did not experience
134 a significant decrease or even suffered from a slight increase when these redundant ones were
135 removed from the model. At last, a total of 64001 samples and 7 variables were utilized to predict
136 the ambient benzene concentrations at the global scale.

137 2.2 Model development

138 2.2.1 The ensemble model development for atmospheric benzene estimates

139 In the pioneering studies, random forest (RF), extreme gradient boosting (XGBoost), and light
140 gradient boosting machine (LightGBM) exhibited the better estimation accuracy (Li et al., 2021).
141 RF model holds a great deal of decision trees, and each one experiences an independent sampling
142 procedure and all of these trees show the same distributions (Breiman). RF model often displays
143 excellent prediction performance owing to the injected randomness. The model accuracy is strongly
144 dependent on the number of trees, splitting features, and the variable group. The detailed procedures
145 are summarized as follows:



146
$$f(x) = \sum_{z=1}^Z c_z R(x \in Q_z) \quad (1)$$

147
$$c_z = \overset{\Delta}{\text{average}}(y_i | x_i \in Q_z) \quad (2)$$

148
$$BR_1(p, q) = \{X | X_j \leq q\} \& BR_2(p, q) = \{X | X_j > q\} \quad (3)$$

149
$$\min_{p,q} \left[\min_{M_1(p,q)} \sum (y - c_1)^2 + \min_{M_2(p,q)} \sum (y - c_2)^2 \right] \quad (4)$$

150
$$c_1 = \overset{\Delta}{\text{average}}(y_i | x_i \in Q_1(p, q)) \& c_2 = \overset{\Delta}{\text{average}}(y_i | x_i \in Q_2(p, q)) \quad (5)$$

151 where (x_i, y_i) is the sample for $i = 1, 2, \dots, N$ in Q regions (Q_1, Q_2, \dots, Q_Z) ; R denotes the weight
 152 of each branch; BR represents decision tree branch; c_m is the response to the model; $\overset{\Delta}{c}_z$ represents
 153 the optimal value, p is the feature variable; c_1 is the average of left branch; c_2 is the average of right
 154 branch; q represents the split point.

155 XGBoost model is an improved algorithm of gradient boosting decision tree (GBDT) model and
 156 loss functions have been extended to the second order function. The detailed XGBoost algorithm is
 157 shown as the following formula (Zhai and Chen, 2018):

158
$$Y^{(t)} = \sum_{i=1}^n [l(y_i, \overset{\Delta}{y}^{(t-1)}) + \partial_{\overset{\Delta}{y}^{(t-1)}} l(y_i, \overset{\Delta}{y}^{(t-1)}) f_t(x_i) + \frac{1}{2} \partial_{\overset{\Delta}{y}^{(t-1)}}^2 l(y_i, \overset{\Delta}{y}^{(t-1)}) f_t^2(x_i)] + \varepsilon(f_t) \quad (6)$$

159 where $Y^{(t)}$ is the cost function at the t -th period; ∂ represents the derivative of the original function;
 160 $\partial_{\overset{\Delta}{y}^{(t-1)}}^2$ is the second derivative of the original function; l is the differentiable convex loss function
 161 that reflects the minus of the predicted value ($\overset{\Delta}{y}$) of the i -th instance at the t -th period and the target
 162 value (y_i); $f_t(x)$ represents the increment; $\varepsilon(f_t)$ is the regularizer.

163 LightGBM model is an update version of XGBoost method, and significantly improve the
 164 running speed of modelling process. Moreover, this method could decrease the cache miss by a large
 165 margin and further improved the predictive accuracy. The detailed algorithms are as follows (Sun
 166 et al., 2020):

167
$$\overset{\Delta}{f} = \arg \min_f L(y, f(x)) \quad (7)$$



168
$$f_T(X) = \sum_{i=1}^T f_i(X) \quad (8)$$

169
$$\Gamma_i = \sum_{i=1}^n (g_i f_i(x_i) + \frac{1}{2} h_i f_i^2(x_i)) \quad (9)$$

170 where \hat{f} is the least value of cost function; $L(y, f(x))$ is the cost function; $f_T(X)$ denotes the total
171 regression trees; $f_i(X)$ represents each regression tree; g_i and h_i represent the first- and second-order
172 gradient statistics of the cost function, respectively.

173 Although all of these models showed the better performance in predicting air pollutants, nearly
174 all of these submodels still suffered from some weaknesses in the prediction accuracy. Hence, it was
175 necessary to collocate these models using back-propagation neural network (BPNN) to further
176 simulate daily ambient benzene concentrations at the global scale. As depicted in Figure 1, three
177 submodels including RF, XGBoost, and LightGBM were stacked through BPNN model to simulate
178 the daily atmospheric benzene levels at the global scale. Firstly, a 5-fold cross-validation method
179 was utilized to train each submodel to determine the optimal hyperparameter. Then, the BPNN
180 method was employed to further train the estimated concentrations of three submodels against the
181 observations (Figure 1). Lastly, the global ambient benzene concentrations were predicted on the
182 basis of the ensemble model.

183 2.2.2 The meteorology-normalized benzene estimates

184 The ambient benzene concentration was influenced by both of meteorological parameters and
185 emissions. To isolate the contribution of emission, the impacts of meteorological conditions should
186 be removed. In our study, the XGBoost approach was utilized to eliminate the impacts of
187 meteorological conditions. The simulated benzene concentration in each grid (0.25°) based on the
188 method in section 2.2.1 was treated as the dependent variable. The daily benzene emission,
189 meteorological factors, month of year (MOY), and day of year (DOY) in each grid were regarded
190 as the explanatory variables. The raw dataset was randomly classified into a training dataset (90%
191 of input dataset) for developing the XGBoost model and the remained samples were regarded as the
192 test dataset. After the development of the XGBoost model, the weather normalized technique was
193 employed to predict the ambient benzene concentration at a specific time point. The detailed
194 deweathered algorithms was introduced by Grange and Carslaw (2019) firstly. The meteorology-



195 normalized benzene level served as the concentrations contributed by emission alone. The
196 differences of total and deweathered benzene concentrations were regarded as the concentration
197 contributed by meteorology. In addition, the CV R^2 value of model using for the separation of
198 meteorology and emission also should be higher than 0.50, otherwise the model could be considered
199 to be unreliable.

200 2.3 Health effect assessment

201 In our study, the carcinogenic and non-carcinogenic risks of ambient benzene were assessed
202 based on the standard methodology of United States Environmental Protection Agency (USEPA).
203 The carcinogenic and non-carcinogenic risks induced by benzene exposure for were evaluated based
204 on the lifetime carcinogenic risks (LCR) and hazard index (HI). The formulas for calculating
205 benzene intake (BI), LCR, and HI are as follows (Table S1):

$$206 \quad BI = (C \times ET \times EF \times ED) / (365 \times 24 \times AT) \quad (10)$$

$$207 \quad HI = BI / RfC \quad (11)$$

$$208 \quad LCR = BI \times IUR \quad (12)$$

209 where C ($\mu\text{g}/\text{m}^3$) denotes the concentration of the corresponding ambient benzene; ET is the
210 exposure time; EF represents the annual exposure frequency (d a^{-1}); ED is the exposure duration
211 (a); AT_{nca} and AT_{ca} denotes the average exposure time for carcinogenic and non-carcinogenic risks
212 (a), respectively. BI means the benzene intake; RfC represents the reference dose ($\mu\text{g}/\text{m}^3$); IUR is
213 the inhalation risk ($1/\mu\text{g}/\text{m}^3$). The non-carcinogenic risk of the ambient benzene is considered to be
214 high when HI was above 1.0, whereas the health risk is not obvious when HI is below 1.0. The
215 carcinogenic risk was regarded as definite risk when LCR was higher than 1×10^{-4} , while it was
216 treated as the possible risk when this indicator was located between 1×10^{-6} and 1×10^{-4} . The risk
217 was treated as negligible when the indicator was lower than 1×10^{-6} (Dumanoglu et al., 2014; Li et
218 al., 2017).

219 3. Results and discussion

220 3.1 The model fitting and validation

221 The ensemble model was utilized to estimate the ambient benzene concentrations at the global scale
222 during 23 January-30 June in 2019 and 2020. The cross-validation (CV) R^2 value of the ensemble
223 model ($R^2 = 0.60$) was significantly higher than that of RF (0.52), XGBoost (0.53), and LightGBM



224 (0.55) (Figure S3). Nevertheless, both of the root-mean-square error (RMSE) ($1.18 \mu\text{g}/\text{m}^3$) and the
225 mean absolute error (MAE) ($0.59 \mu\text{g}/\text{m}^3$) of the ensemble model were significantly lower than those
226 of RF (RMSE and MAE: 1.41 and $0.72 \mu\text{g}/\text{m}^3$), XGBoost (RMSE and MAE: 1.37 and $0.70 \mu\text{g}/\text{m}^3$),
227 and LightGBM (RMSE and MAE: 1.34 and $0.69 \mu\text{g}/\text{m}^3$). The higher R^2 value and the lower RMSE
228 and MAE suggested the higher accuracy of the ensemble model in air quality simulation. In the
229 pioneering studies, Wolpert (1992) confirmed that the joint use of multiple statistical models could
230 decrease the probability of overfitting and strengthen the predictive accuracy and transferability of
231 final models. Besides, our previous studies also demonstrated that the stacking of various decision
232 tree models could significantly outperform individual model because each decision tree model could
233 suffer from some weaknesses (Li et al., 2021). For instance, the dataset in the RF model appeared
234 to be over-fitted when much noise existed in the training data of regression problems (Breiman,
235 2001). Besides, RF model might underestimated/overestimated the extremely values of ambient
236 benzene (Xue et al., 2019), which could be neutralized by the XGBoost algorithm through the
237 boosting method (Li et al., 2020). For XGBoost algorithm, excessive leaf nodes often showed low
238 splitting gain, while the LightGBM model could make up this defect (Nemeth et al., 2019). Overall,
239 the combination of these decision tree models could overcome these weaknesses of these individual
240 models and enhance the robustness of the final model.

241 Although 10-fold CV has verified that the modelling performance of ensemble model was
242 superior to the individual models, this method cannot examine the spatial transferability of this
243 model. In our study, many regions except India, Europe, and the United States were lack of
244 monitoring sites of ambient benzene. Fortunately, the CTMs output provided a strong proxy to
245 predict the daily ambient benzene concentrations before and after COVID-19 outbreak. In order to
246 test the spatial extrapolation of the ensemble model, the site-based validation was performed. In
247 each round, two-thirds of the dataset in India, Europe, and the United States were applied to train
248 the model and the remained one was utilized to examine the model (e.g., India+Europe for training
249 and the United States for testing). After three rounds, all of the simulated benzene concentrations
250 were compared with the corresponding observed values. As shown in Figure S4, the out-of-bag R^2
251 value reached 0.58, which was slightly lower than the R^2 value (0.60) of training model. In addition,
252 RMSE and MAE of the fitting equation for the out-of-bag data were 1.18 and 0.62, respectively.



253 The result was in good agreement with those based on CV database, indicating the ensemble model
254 showed satisfied spatial generalization.

255 The ensemble model can capture the spatiotemporal variation of ambient benzene during
256 COVID-19 lockdown period, while the impact of COVID-19 lockdown cannot be quantified
257 because the contribution of meteorological parameters cannot be removed based on this model alone.
258 Therefore, it is proposed to employ the XGBoost algorithm to isolate the contribution of emission
259 reduction to global atmospheric benzene. As depicted in Figure S5, the CV R^2 value and slope of
260 fitting curve reached 0.65 and 0.62, respectively. The result suggested that meteorology-normalized
261 model was robust because the CV R^2 value was much higher than 0.50.

262 3.2 The impact of COVID-19 lockdown on global atmospheric benzene level

263 The ensemble model was developed to expand the ground-observed benzene measurement to
264 the global scale and capture the global spatial variability of ambient benzene. As shown in Figure
265 S6, the global simulated (total) benzene concentration during Jan. 23-Jun. 30 in 2019 and 2020
266 ranged from 0.52 to 6.36 $\mu\text{g}/\text{m}^3$, with the average value of $0.92 \pm 0.23 \mu\text{g}/\text{m}^3$. At the regional scale,
267 the benzene concentration displayed significantly spatial variability. The benzene concentration
268 followed the order of India ($1.44 \pm 0.14 \mu\text{g}/\text{m}^3$) > China ($1.17 \pm 0.13 \mu\text{g}/\text{m}^3$) > Europe (1.02 ± 0.08
269 $\mu\text{g}/\text{m}^3$) > United States ($0.96 \pm 0.09 \mu\text{g}/\text{m}^3$) during Jan. 23-Jun. 30 in 2019 and 2020. Besides, the
270 global simulated mean benzene level suffered from slight decrease from 0.93 ± 0.06 in 2020 to 0.90
271 ± 0.06 in 2019. However, the inter-annual variation of ambient benzene exhibited remarkable spatial
272 discrepancy at the global scale. As depicted in Figure S7, the change ratio of simulated (total)
273 benzene level during the COVID-19 lockdown period (the difference of the benzene level before
274 COVID-19 lockdown and that during COVID-19 lockdown period) in 2020 was in the order of
275 India (-18.5%) > Europe (-16.7%) > China (-11.7%) > United States (-11.5%). Compared with 2020,
276 the change ratio of benzene level during the same period in 2019 followed the order of India (-
277 16.3%) > Europe (-6.62%) > United States (-6.46%) > China (-4.18%). It should be noted that the
278 simulated ambient benzene concentration suffered from the higher decreasing ratio in 2020
279 compared with the same period in 2019 in nearly all of the major countries around the world, which
280 might be associated with the local COVID-19 lockdown measures in 2020.

281 Due to the interference of meteorological conditions, we cannot quantify the direct impact of



282 COVID-19 lockdown on ambient benzene based on the comparison of simulated (total) benzene
283 levels. Thus, the meteorology-normalized method was employed to decouple the separated
284 contributions of emission reduction and meteorology to ambient benzene. In our study, both of the
285 change ratio and detrended change ratio were applied to evaluate the impact of COVID-19
286 lockdown on global ambient benzene level. The change ratio represents the variation of ambient
287 benzene level during lockdown period in 2020 compared with pre-lockdown period in 2020.
288 However, the detrended change ratio reflects the difference of the change ratio in 2020 and the
289 change ratio during the same period in 2019, which could avoid the inter-annual system error and
290 contingency of a single year. As summarized in Figure 2 and 3, the change ratio of deweathered
291 benzene concentration from pre-lockdown to lockdown period in 2020 was in the order of India (-
292 23.6%) > Europe (-21.9%) > United States (-16.2%) > China (-15.6%). Meanwhile, the change ratio
293 of deweathered benzene concentration during the same time in 2019 followed the order of Europe
294 (-10.2%) > United States (-8.04%) > India (-7.40%) > China (-2.31%). The large gap in the change
295 ratio of deweathered benzene level between 2019 and 2020 confirmed that the drastic and
296 consequential quarantines significantly decreased the ambient benzene concentrations in nearly all
297 of the regions with lockdown measures. Among all of the major countries, India suffered from the
298 most dramatic benzene decrease during 24 March 2020-24 April 2020 (-23.6%) compared with the
299 same period in 2019 (-7.4%). During this period, the prohibition of industrial activities and mass
300 transportation was proposed to curb the spread of COVID-19 pandemic, leading to the tremendous
301 reduction of anthropogenic benzene emission (Pathakoti et al., 2021; Zhang et al., 2021). The
302 decrease ratio of deweathered benzene level in India was close to that of PM_{2.5} (-26%), while it is
303 was markedly lower than that of NO₂ (-50%) (Zhang et al., 2021). Although both of Europe and the
304 United States also performed stringent lockdown restrictions in some regions such as Italy, Spain,
305 and California (Guevara et al., 2021a; Keller et al., 2021a), while the detrended change (P*: change
306 ratio in 2020-change ratio in 2019) for deweathered benzene in Europe (P* = -13.9%) and the United
307 States (P* = -6%) between 2020 and 2019 was still lower than that of India (P* = -16.2%) (Table
308 1). It was assumed that the absolute concentration of ambient benzene in Europe and the United
309 States were much lower than that in India. It should be noted that the China displayed relatively
310 gentle decreasing ratio (-15.6%) after COVID-19 outbreak, which was even lower than the ratio in



311 the United States. As the first epidemic epicenter country, Chinese government imposed a rapid
312 lockdown measure in Wuhan and other cities across China in an effort to prevent the spread of the
313 COVID-19 pandemic (Wu et al., 2020). These restrictions interrupted a wide array of economic
314 activities and reduced primary air pollutant emissions, and thus resulted in the remarkable decreases
315 of deweathered NO₂ (-43.6%) and PM_{2.5} (-22%) (Dai et al., 2021). The gentle decreasing ratio of
316 ambient benzene compared with other pollutants might be linked with the source apportionment of
317 atmospheric benzene. It was well known that industrial source (e.g., chemical industry and solvent
318 use) was major emission sector of benzene (Li et al., 2019). Although the contribution from solvent
319 use exhibited substantial decreases in some cities (Qi et al., 2021; Wang et al., 2021), the chemical
320 industry was not entirely interrupted even during the COVID-19 lockdown period (Dai et al., 2021).
321 Zheng et al. (2021a) also demonstrated that the reduction of non-methane volatile organic
322 compounds (NMVOCs) emission from industry sector was much less than other pollutants.

323 Although the deweathered benzene concentrations in nearly all of the major countries
324 experienced obvious decreases during COVID-19 lockdown period, the change ratios of
325 deweathered benzene in different regions of these countries still showed large spatial variability. In
326 China, most of the cities in East China such as Beijing (-30.6%), Shanghai (-6.25%), and Wuhan (-
327 45.3%) experienced dramatic decreases of deweathered benzene levels (Figure S8), which was
328 mainly contributed by the simultaneous emission reduction of industry and transportation sectors.
329 However, the deweathered benzene concentrations in Northeast China and Yunnan province even
330 exhibited slight increases after COVID-19 outbreak (Figure 4). Dai et al. (2021) also found that the
331 deweathered PM_{2.5} concentration in Kunming increased ~20% after COVID-19 outbreak. At first,
332 the contribution of residential combustion source (62.1%) to atmospheric benzene in Yunnan
333 province was higher than other sectors (Guevara et al., 2021b; Kuenen et al., 2021). Moreover, the
334 increase of domestic emission due to home quarantine order further increased the ambient benzene
335 concentration (10%) in this province, which has been demonstrated by the updated emission
336 inventory in 2020 (Dolumbia et al., 2021). The slight increases of deweathered benzene levels in
337 Northeast China after COVID-19 outbreak could be linked with the earlier work
338 resumption(<https://baijiahao.baidu.com/s?id=1658138056285012986&wfr=spider&for=pc>). Based
339 on the simulation result, the deweathered ambient benzene level in Northeast China rebounded



340 sharply after the third week, and then returned back to normal in the late February. In India, the
341 decreasing ratios of deweathered benzene in Delhi, Mumbai, Kolkata, Bengaluru, Hyderabad,
342 Chennai, Ahmedabad, and Lucknow reached 21.6%, 20.9%, 73.7%, 26.9%, 38.0%, 33.7%, 25.1%,
343 and 33.3% during COVID-19 lockdown period (Figure S9), respectively. In Europe, the
344 deweathered benzene levels in nearly all of the cities displayed marked decreases because most
345 European countries have imposed lockdowns to combat the spread of the COVID-19 pandemic
346 (Guevara et al., 2021a). For instance, the private car use and heavy good vehicles (HGVs) on the
347 road in London reduced by 80% and 30-40%, respectively (Shi et al., 2021). The substantial
348 reduction of transportation emission triggered the P* value in London between 2020 and 2019
349 reaching -43.6%. In the United States, the decreasing ratios of meteorology-normalized benzene
350 levels in the cities of Eastern United States and California were generally higher than those in
351 Central United States, which was in good agreement with the spatial variability of PM_{2.5} decrease
352 (Hammer et al., 2021).

353 In addition, ambient benzene levels were also strongly affected by meteorological conditions
354 that alter photochemical production, advection, and depositional loss. Hence, we examined how
355 meteorological parameters influenced the temporal variability of ambient benzene during COVID-
356 19 lockdown period. In 2020, most of the major countries including China (3.90%), Europe (5.20%),
357 and the United States (4.70%) suffered from slight unfavorable meteorological conditions, which
358 was in good agreement with the impact of meteorological conditions on ambient NO₂ concentrations
359 (Shi et al., 2021). The result suggested that the unfavorable meteorological conditions weakened the
360 health benefits of ambient benzene due to drastic lockdown measures around the world.

361 3.3 The effect of COVID-19 lockdown on global health risks

362 The global average LCR during 23 January-30 June in 2019 and 2020 were 4.89×10^{-7} and
363 4.51×10^{-7} after removing the contributions of meteorological conditions, respectively (Figure S10).
364 Although the COVID-19 lockdown decreased the LCR value slightly, both of the LCR values during
365 two periods were lower than the threshold level of 10^{-6} , suggesting that dwellings in most regions
366 could avoid carcinogenic risk through inhalation exposure to benzene (Li et al., 2017). However,
367 the LCR values showed significant spatial difference in different regions. For instance, North China
368 often suffered from the relatively higher benzene pollution, and the LCR value in this region



369 decreased from 1.03×10^{-6} (possible risk) during the study period in 2019 (the same period to 2020)
370 to 7.37×10^{-7} during COVID-19 lockdown period. The result verified that the stringent emission
371 control measures significantly decreased the health risk due to benzene exposure. The LCR value
372 across India only decreased from 6.55×10^{-7} to 6.42×10^{-7} during the study period, whereas the
373 northern part of India such as Bihar decreased from 1.14×10^{-6} to 1.09×10^{-6} due to the impact of
374 COVID-19 lockdown (Figure 5). As the most populous province of India, Bihar possessed more
375 than 124 million people (<http://kolkata.china-consulate.org/chn/lqgk/t1331638.htm>). The result
376 suggested that the COVID-19 lockdown certainly obtained remarkable short-term health benefits
377 through decreasing the ambient benzene exposure. The LCR values in Europe and the United States
378 decreased from 4.99×10^{-7} and 4.77×10^{-7} to 4.57×10^{-7} and 4.63×10^{-7} , respectively. Compared
379 with China and India, Europe and the United States suffered from relatively low carcinogenic risk
380 of benzene exposure even before COVID-19 lockdown. Although the COVID-19 lockdown further
381 decreased the LCR values in these regions, the overall carcinogenic risk was negligible.

382 Additionally, the non-carcinogenic risk around the world during the period was also assessed
383 based on HI. The average HI of ambient benzene exposure in China, India, Europe, and the United
384 States reduced from 8.92×10^{-3} , 7.45×10^{-3} , 6.32×10^{-3} , and 5.76×10^{-3} in 2019 to 8.53×10^{-3} ,
385 7.13×10^{-3} , 5.81×10^{-3} , and 5.59×10^{-3} during COVID-19 lockdown period in 2020 (Figure 6),
386 respectively. Although HI value in some regions including Bihar (1.52×10^{-2} to 1.41×10^{-2}) and
387 Uttar Pradesh (1.04×10^{-2} to 1.03×10^{-2}) in India and Beijing-Tianjin-Hebei (BTH) (1.25×10^{-2} to
388 1.14×10^{-2}) in China still experienced decreases during COVID-19 lockdown period, the HI values
389 in these regions were still significantly lower than the risk threshold (HI = 1). Therefore, the impact
390 of COVID-19 lockdown on non-carcinogenic risk of benzene exposure was insignificant.

391 **4. Conclusions and implications**

392 The drastic lockdown measures largely reduced the air pollutant emissions. The meteorology-
393 normalized ambient benzene concentrations in China (-15.6%), India (-23.6%), Europe (-21.9%),
394 and the United States (-16.2%) experienced dramatic decreases after COVID-19 outbreak.
395 Furthermore, the decreasing ratios in these major regions during COVID-19 lockdown period were
396 much higher than the same period in 2019, indicating the aggressive emission reduction measures
397 efficiently decreased ambient benzene concentrations. Emission reductions from industrial activities



398 and transportation were major drivers for the decreasing of ambient benzene level during lockdown
399 period, while the relatively stable solvent use emission could restrict the further decrease of benzene
400 pollution. Besides, the slight increase of domestic emission during this period might be an important
401 reason for the benzene increase in some regions (e.g., Yunnan province). There is also an urgent
402 need to control the household combustion and solvent use emissions apart from the emissions from
403 industry and transportation sectors.

404 Besides, substantial decreases of atmospheric benzene levels could save sufficient health
405 benefits. Dramatic decreases of benzene emissions in Europe and the United States cannot save
406 effective health benefits because the ambient benzene levels in both of these regions during
407 business-as-usual scenario were significantly lower than the risk threshold. In contrast, the benzene
408 decreases in North China Plain (NCP), China and Bihar, India could save abundant health benefits
409 because these regions often suffered from severe atmospheric benzene pollution during business-
410 as-usual scenario. Thus, more targeted abatement measures are needed to reduce the benzene
411 emission in these areas.

412 **Acknowledgements**

413 This work was supported by the National Natural Science Foundation of China (42107113).

414 **Data availability**

415 The CEDS emission inventory are available at the website of
416 <https://zenodo.org/record/3754964#.YwrJL8jfmfU>. The global meteorological parameters
417 (reanalysis dataset) are obtained from the website of <http://geoschemdata.wustl.edu/ExtData/>.

418 **Author contributions**

419 LCH and LR wrote the manuscript. LR and CLL contributed to the conceptualization of the study.
420 LCH and LR conducted the research, and visualized the results. CLL revised the manuscript.

421 **Competing interests**

422 The contact author has declared that neither they nor their co-authors have any competing interests.

423



424 **References**

- 425 Bauwens, M., Compemolle, S., Stavrakou, T., Müller, J.-F., van Gent, J., Eskes, H., Levelt, P.F., van der
426 A, R., Veeffkind, J.P., Vlietinck, J., Yu, H., Zehner, C. (2020) Impact of Coronavirus Outbreak on NO₂
427 Pollution Assessed Using TROPOMI and OMI Observations. *Geophysical Research Letters* 47,
428 e2020GL087978.
- 429 Berg, K., Romer Present, P., Richardson, K. (2021) Long-term air pollution and other risk factors
430 associated with COVID-19 at the census tract level in Colorado. *Environmental pollution* 287, 117584.
- 431 Bocquet, M., Elbern, H., Eskes, H., Hirtl, M., Žabkar, R., Carmichael, G., Flemming, J., Inness, A.,
432 Pagowski, M., Pérez Camaño, J. (2015) Data assimilation in atmospheric chemistry models: current
433 status and future prospects for coupled chemistry meteorology models. *Atmospheric Chemistry and*
434 *Physics* 15, 5325-5358.
- 435 Breiman, L. (2001) Random forests. *Machine learning* 45, 5-32.
- 436 Chang, Y., Huang, R.J., Ge, X., Huang, X., Hu, J., Duan, Y., Zou, Z., Liu, X., Lehmann, M.F. (2020)
437 Puzzling haze events in China during the coronavirus (COVID-19) shutdown. *Geophysical Research*
438 *Letters* 47, e2020GL088533.
- 439 Cui, L., Li, R., Zhang, Y., Meng, Y., Zhao, Y., Fu, H. (2019) A geographically and temporally weighted
440 regression model for assessing intra-urban variability of volatile organic compounds (VOCs) in
441 Yangpu district, Shanghai. *Atmospheric Environment* 213, 746-756.
- 442 Dai, Q., Hou, L., Liu, B., Zhang, Y., Song, C., Shi, Z., Hopke, P.K., Feng, Y. (2021) Spring Festival and
443 COVID-19 lockdown: disentangling PM sources in major Chinese cities. *Geophysical Research*
444 *Letters*, e2021GL093403.
- 445 Dombia, T., Granier, C., Elguindi, N., Bouarar, I., Darras, S., Brasseur, G., Gaubert, B., Liu, Y., Shi, X.,
446 Stavrakou, T. (2021) Changes in global air pollutant emissions during the COVID-19 pandemic: a
447 dataset for atmospheric modeling. *Earth System Science Data* 13, 4191-4206.
- 448 Dumanoglu, Y., Kara, M., Altioik, H., Odabasi, M., Elbir, T., Bayram, A. (2014) Spatial and seasonal
449 variation and source apportionment of volatile organic compounds (VOCs) in a heavily industrialized
450 region. *Atmospheric Environment* 98, 168-178.
- 451 Geddes, J.A., Martin, R.V., Boys, B.L., van Donkelaar, A. (2016) Long-term trends worldwide in ambient
452 NO₂ concentrations inferred from satellite observations. *Environmental health perspectives* 124, 281-
453 289.
- 454 Grange, S.K., Carslaw, D.C. (2019) Using meteorological normalisation to detect interventions in air
455 quality time series. *Science of the Total Environment* 653, 578-588.
- 456 Guevara, M., Jorba, O., Soret, A., Petetin, H., Bowdalo, D., Serradell, K., Tena, C., Denier van der Gon,
457 H., Kuenen, J., Peuch, V.-H. (2021a) Time-resolved emission reductions for atmospheric chemistry
458 modelling in Europe during the COVID-19 lockdowns. *Atmospheric Chemistry and Physics* 21, 773-
459 797.
- 460 Guevara, M., Jorba, O., Tena, C., Denier van der Gon, H., Kuenen, J., Elguindi, N., Darras, S., Granier,
461 C., Pérez García-Pando, C. (2021b) Copernicus Atmosphere Monitoring Service TEMPOral profiles
462 (CAMs-TEMPO): global and European emission temporal profile maps for atmospheric chemistry
463 modelling. *Earth System Science Data* 13, 367-404.
- 464 Gurjar, B.R., Ravindra, K., Nagpure, A.S. (2016) Air pollution trends over Indian megacities and their
465 local-to-global implications. *Atmospheric Environment* 142, 475-495.
- 466 Hammer, M.S., van Donkelaar, A., Martin, R.V., McDuffie, E.E., Lyapustin, A., Sayer, A.M., Hsu, N.C.,
467 Levy, R.C., Garay, M.J., Kalashnikova, O.V. (2021) Effects of COVID-19 lockdowns on fine



- 468 particulate matter concentrations. *Science Advances* 7, eabg7670.
- 469 Hsu, C.-Y., Chiang, H.-C., Shie, R.-H., Ku, C.-H., Lin, T.-Y., Chen, M.-J., Chen, N.-T., Chen, Y.-C. (2018)
- 470 Ambient VOCs in residential areas near a large-scale petrochemical complex: Spatiotemporal
- 471 variation, source apportionment and health risk. *Environmental Pollution* 240, 95-104.
- 472 Hu, L., Keller, C.A., Long, M.S., Sherwen, T., Auer, B., Da Silva, A., Nielsen, J.E., Pawson, S.,
- 473 Thompson, M.A., Trayanov, A.L. (2018) Global simulation of tropospheric chemistry at 12.5 km
- 474 resolution: performance and evaluation of the GEOS-Chem chemical module (v10-1) within the
- 475 NASA GEOS Earth system model (GEOS-5 ESM). *Geoscientific Model Development* 11, 4603-4620.
- 476 Huang, X., Ding, A., Gao, J., Zheng, B., Zhou, D., Qi, X., Tang, R., Wang, J., Ren, C., Nie, W. (2021)
- 477 Enhanced secondary pollution offset reduction of primary emissions during COVID-19 lockdown in
- 478 China. *National Science Review* 8, nwaal37.
- 479 Ivatt, P.D., Evans, M.J. (2020) Improving the prediction of an atmospheric chemistry transport model
- 480 using gradient-boosted regression trees. *Atmos. Chem. Phys.* 20, 8063-8082.
- 481 Kamal, M.S., Razzak, S.A., Hossain, M.M. (2016) Catalytic oxidation of volatile organic compounds
- 482 (VOCs)—A review. *Atmospheric Environment* 140, 117-134.
- 483 Keller, C.A., Evans, M.J., Knowland, K.E., Hasenkopf, C.A., Modekurty, S., Lucchesi, R.A., Oda, T.,
- 484 Franca, B.B., Mandarino, F.C., Diaz Suárez, M.V. (2021a) Global impact of COVID-19 restrictions
- 485 on the surface concentrations of nitrogen dioxide and ozone. *Atmospheric Chemistry and Physics* 21,
- 486 3555-3592.
- 487 Keller, C.A., Knowland, K.E., Duncan, B.N., Liu, J., Anderson, D.C., Das, S., Lucchesi, R.A., Lundgren,
- 488 E.W., Nicely, J.M., Nielsen, E. (2021b) Description of the NASA GEOS Composition Forecast
- 489 Modeling System GEOS-CF v1. 0. *Journal of Advances in Modeling Earth Systems* 13,
- 490 e2020MS002413.
- 491 Kim, K.-H., Jahan, S.A., Kabir, E. (2013) A review on human health perspective of air pollution with
- 492 respect to allergies and asthma. *Environment international* 59, 41-52.
- 493 Koppmann, R. (2008) Volatile organic compounds in the atmosphere. John Wiley & Sons.
- 494 Kuenen, J., Dellaert, S., Visschedijk, A., Jalkanen, J.-P., Super, I., Denier van der Gon, H. (2021) CAMS-
- 495 REG-v4: a state-of-the-art high-resolution European emission inventory for air quality modelling.
- 496 *Earth System Science Data Discussions*, 1-37.
- 497 Li, B., Ho, S.S.H., Xue, Y., Huang, Y., Wang, L., Cheng, Y., Dai, W., Zhong, H., Cao, J., Lee, S. (2017)
- 498 Characterizations of volatile organic compounds (VOCs) from vehicular emissions at roadside
- 499 environment: The first comprehensive study in Northwestern China. *Atmospheric Environment* 161,
- 500 1-12.
- 501 Li, M., Zhang, Q., Zheng, B., Tong, D., Lei, Y., Liu, F., Hong, C., Kang, S., Yan, L., Zhang, Y. (2019)
- 502 Persistent growth of anthropogenic non-methane volatile organic compound (NMVOC) emissions in
- 503 China during 1990–2017: drivers, speciation and ozone formation potential. *Atmospheric Chemistry*
- 504 *and Physics* 19, 8897-8913.
- 505 Li, R., Cui, L., Fu, H., Zhao, Y., Zhou, W., Chen, J. (2020) Satellite-Based Estimates of Wet Ammonium
- 506 (NH₄-N) Deposition Fluxes Across China during 2011–2016 Using a Space–Time Ensemble Model.
- 507 *Environmental science & technology* 54, 13419-13428.
- 508 Li, R., Cui, L., Zhao, Y., Zhou, W., Fu, H. (2021) Long-term trends of ambient nitrate (NO₃-)
- 509 concentrations across China based on ensemble machine-learning models. *Earth System Science Data*
- 510 13, 2147-2163.
- 511 Ling, C., Li, Y. (2021) Substantial changes of gaseous pollutants and health effects during the COVID-



- 512 19 lockdown period across China. *GeoHealth*, e2021GH000408.
- 513 Liu, H., Gong, P., Wang, J., Clinton, N., Bai, Y., Liang, S. (2020) Annual dynamics of global land cover
514 and its long-term changes from 1982 to 2015. *Earth Syst. Sci. Data* 12, 1217-1243.
- 515 Long, M., Yantosca, R., Nielsen, J., Keller, C., Da Silva, A., Sulprizio, M., Pawson, S., Jacob, D. (2015)
516 Development of a grid-independent GEOS-Chem chemical transport model (v9-02) as an atmospheric
517 chemistry module for Earth system models. *Geoscientific Model Development* 8, 595-602.
- 518 Lu, F., Li, S., Shen, B., Zhang, J., Liu, L., Shen, X., Zhao, R. (2020) The emission characteristic of VOCs
519 and the toxicity of BTEX from different mosquito-repellent incenses. *Journal of hazardous materials*
520 384, 121428.
- 521 Mahato, S., Pal, S., Ghosh, K.G. (2020) Effect of lockdown amid COVID-19 pandemic on air quality of
522 the megacity Delhi, India. *Science of the Total Environment* 730, 139086.
- 523 Mor, S., Kumar, S., Singh, T., Dogra, S., Pandey, V., Ravindra, K. (2021) Impact of COVID-19 lockdown
524 on air quality in Chandigarh, India: understanding the emission sources during controlled
525 anthropogenic activities. *Chemosphere* 263, 127978.
- 526 Mozaffar, A., Zhang, Y.-L. (2020) Atmospheric volatile organic compounds (VOCs) in China: A review.
527 *Current Pollution Reports*, 1-14.
- 528 Nemeth, M., Borkin, D., Michalconok, G., (2019) The comparison of machine-learning methods
529 XGBoost and LightGBM to predict energy development, *Proceedings of the Computational Methods*
530 *in Systems and Software*. Springer, pp. 208-215.
- 531 Pakkattil, A., Muhsin, M., Varma, M.R. (2021) COVID-19 lockdown: Effects on selected volatile organic
532 compound (VOC) emissions over the major Indian metro cities. *Urban Climate* 37, 100838.
- 533 Pathakoti, M., Muppalla, A., Hazra, S., D Venkata, M., A Lakshmi, K., K Sagar, V., Shekhar, R., Jella,
534 S., MV Rama, S.S., Vijayasundaram, U. (2021) Measurement report: An assessment of the impact of
535 a nationwide lockdown on air pollution—a remote sensing perspective over India. *Atmospheric*
536 *Chemistry and Physics* 21, 9047-9064.
- 537 Qi, J., Mo, Z., Yuan, B., Huang, S., Huangfu, Y., Wang, Z., Li, X., Yang, S., Wang, W., Zhao, Y. (2021)
538 An observation approach in evaluation of ozone production to precursor changes during the COVID-
539 19 lockdown. *Atmospheric Environment* 262, 118618.
- 540 Sharma, S., Zhang, M., Anshika, Gao, J., Zhang, H., Kota, S.H. (2020) Effect of restricted emissions
541 during COVID-19 on air quality in India. *Science of the Total Environment* 728, 138878.
- 542 Shi, X., Zhao, C., Jiang, J.H., Wang, C., Yang, X., Yung, Y.L. (2018) Spatial representativeness of PM_{2.5}
543 concentrations obtained using observations from network stations. *Journal of Geophysical Research:*
544 *Atmospheres* 123, 3145-3158.
- 545 Shi, Z., Song, C., Liu, B., Lu, G., Xu, J., Van Vu, T., Elliott, R.J., Li, W., Bloss, W.J., Harrison, R.M.
546 (2021) Abrupt but smaller than expected changes in surface air quality attributable to COVID-19
547 lockdowns. *Science Advances* 7, eabd6696.
- 548 Sun, X., Liu, M., Sima, Z. (2020) A novel cryptocurrency price trend forecasting model based on
549 LightGBM. *Finance Research Letters* 32, 101084.
- 550 Tang, J., Chan, L., Chan, C., Li, Y.S., Chang, C., Liu, S., Wu, D., Li, Y. (2007) Characteristics and diurnal
551 variations of NMHCs at urban, suburban, and rural sites in the Pearl River Delta and a remote site in
552 South China. *Atmospheric Environment* 41, 8620-8632.
- 553 Van Donkelaar, A., Martin, R.V., Brauer, M., Boys, B.L. (2015) Use of satellite observations for long-
554 term exposure assessment of global concentrations of fine particulate matter. *Environmental health*
555 *perspectives* 123, 135-143.



- 556 Wang, M., Lu, S., Shao, M., Zeng, L., Zheng, J., Xie, F., Lin, H., Hu, K., Lu, X. (2021) Impact of COVID-
557 19 lockdown on ambient levels and sources of volatile organic compounds (VOCs) in Nanjing, China.
558 *Science of the Total Environment* 757, 143823.
- 559 Wolpert, D.H. (1992) Stacked generalization. *Neural networks* 5, 241-259.
- 560 Wu, J., Gamber, M., Sun, W., (2020) Does wuhan need to be in lockdown during the Chinese lunar new
561 year? Multidisciplinary Digital Publishing Institute.
- 562 Xue, T., Zheng, Y., Tong, D., Zheng, B., Li, X., Zhu, T., Zhang, Q. (2019) Spatiotemporal continuous
563 estimates of PM_{2.5} concentrations in China, 2000-2016: A machine learning method with inputs from
564 satellites, chemical transport model, and ground observations. *Environment international* 123, 345-
565 357.
- 566 Zhai, B., Chen, J. (2018) Development of a stacked ensemble model for forecasting and analyzing daily
567 average PM_{2.5} concentrations in Beijing, China. *Science of the Total Environment* 635, 644-658.
- 568 Zhang, M., Katiyar, A., Zhu, S., Shen, J., Xia, M., Ma, J., Kota, S.H., Wang, P., Zhang, H. (2021) Impact
569 of reduced anthropogenic emissions during COVID-19 on air quality in India. *Atmospheric Chemistry
570 and Physics* 21, 4025-4037.
- 571 Zheng, B., Zhang, Q., Geng, G., Chen, C., Shi, Q., Cui, M., Lei, Y., He, K. (2021a) Changes in China's
572 anthropogenic emissions and air quality during the COVID-19 pandemic in 2020. *Earth Syst. Sci. Data*
573 13, 2895-2907.
- 574 Zheng, P., Chen, Z., Liu, Y., Song, H., Wu, C.-H., Li, B., Kraemer, M.U.G., Tian, H., Yan, X., Zheng, Y.,
575 Stenseth, N.C., Jia, G. (2021b) Association between coronavirus disease 2019 (COVID-19) and long-
576 term exposure to air pollution: Evidence from the first epidemic wave in China. *Environmental
577 pollution* 276, 116682.
- 578
- 579
- 580
- 581



Figure 1 The workflow of global atmospheric benzene modelling. CTM output represents the simulated benzene concentration based on GEOS-Chem model. Meteo denotes the meteorological parameters derived from GEOS-CF reanalysis. Emission represents the daily emission of benzene. MOY and DOY are the month of year and day of year, respectively. Simulated benzene represents the predicted benzene concentrations based on the ensemble model. Deweathered benzene denotes the benzene concentration after removing meteorological effects.

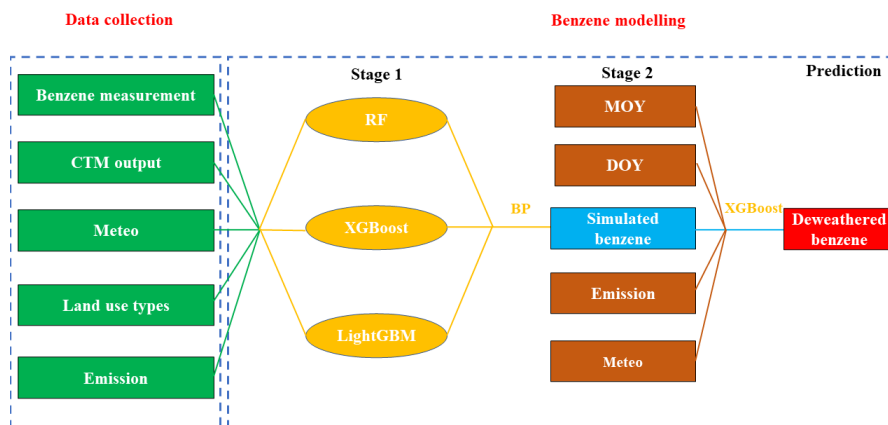




Figure 2 The global average deweathered benzene concentrations in 2019 (Jan. 23-Jun. 30) (a) and 2020 (Jan. 23-Jun. 30) (b). (c) represents the difference of deweathered benzene concentrations in 2020 and 2019.

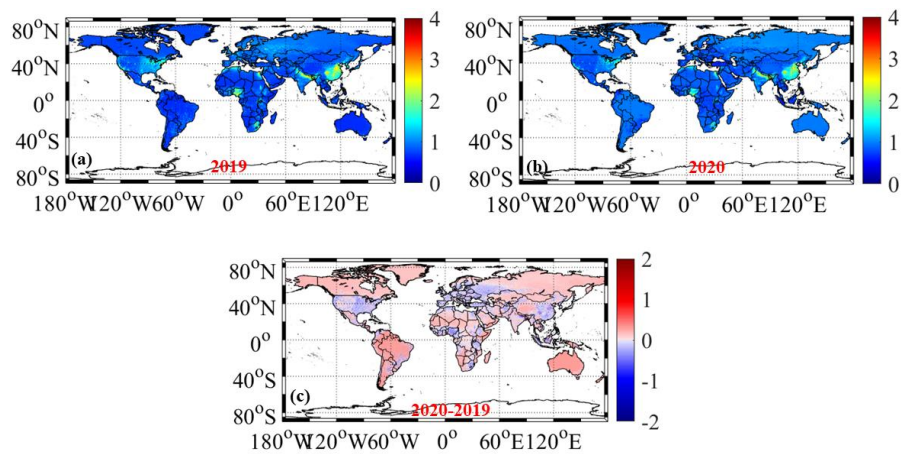




Figure 3 The weekly variations of atmospheric benzene concentrations ($\mu\text{g}/\text{m}^3$) in some major regions around the world during Jan. 23-Jun. 30. The red line and background denote mean values and standard deviation of deweathered weekly benzene concentrations in 2020. The cyan line and background denote mean values and standard deviation of deweathered weekly benzene levels in 2019. The dashed vertical red line suggests COVID-19 restriction dates, and the black line indicates the beginning of easing measures.

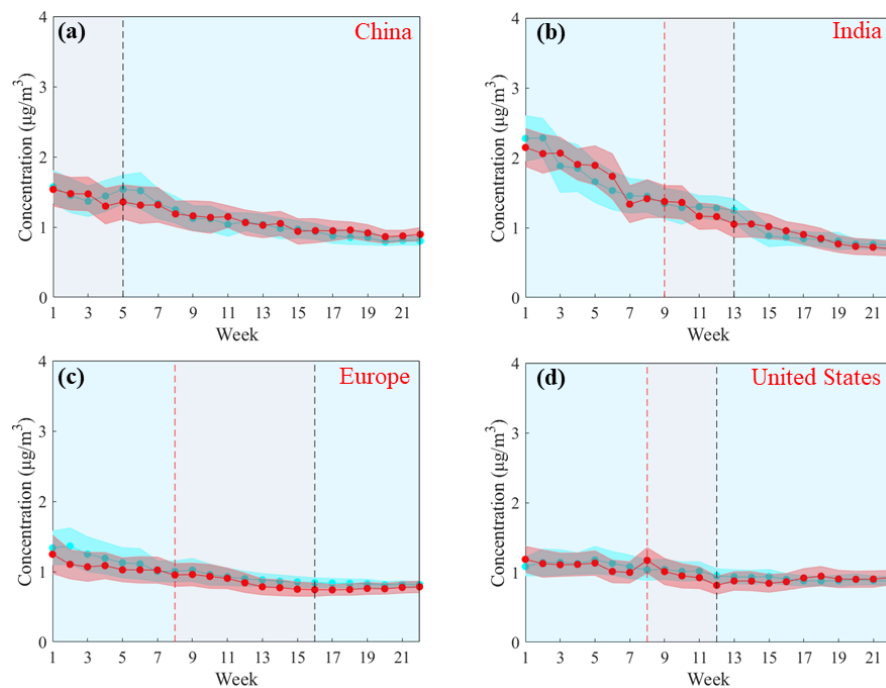




Figure 4 The concentration difference for deweathered benzene between COVID-19 period in 2020 and the same period in 2019 in East Asia, South Asia, Europe, and North America (Difference = deweathered benzene concentration in 2020-deweathered benzene concentration in 2019).

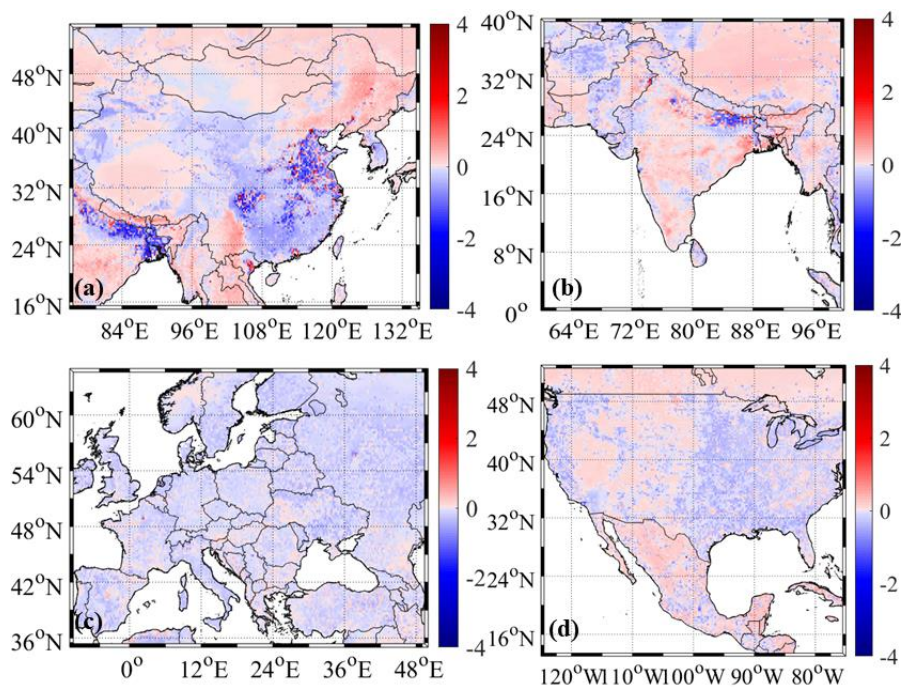




Figure 5 The carcinogenic risk differences (Unit: 10^{-7}) for atmospheric benzene between COVID-19 period in 2020 and the same period in 2019 in East Asia, South Asia, Europe, and North America (Difference = benzene concentration in 2020 - benzene concentration in 2019).

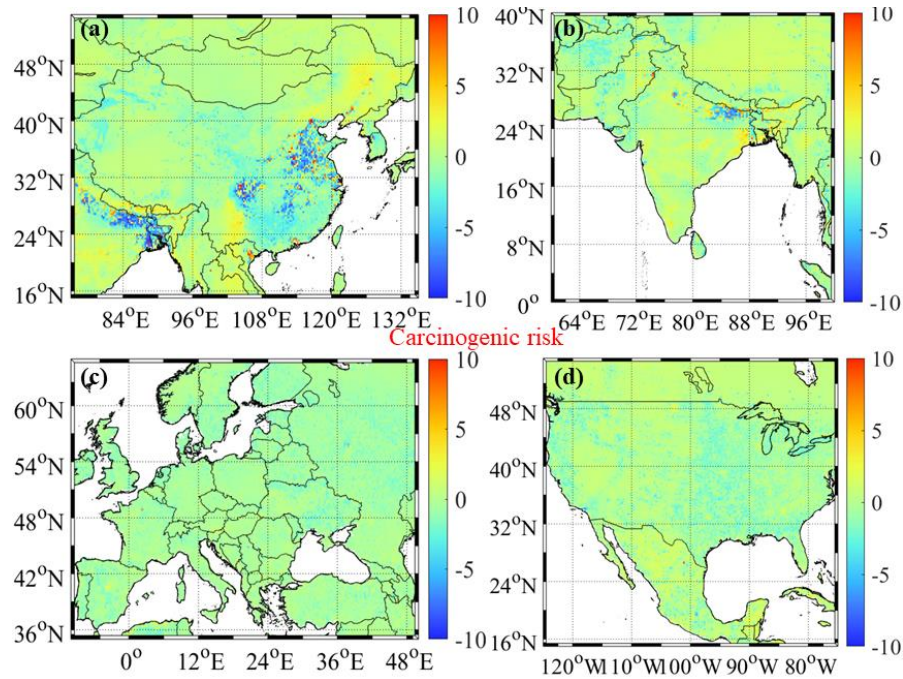




Figure 6 The non-carcinogenic risk differences (Unit: 10^{-3}) for atmospheric benzene between COVID-19 period in 2020 and the same period in 2019 in East Asia, South Asia, Europe, and North America (Difference = benzene concentration in 2020 - benzene concentration in 2019).

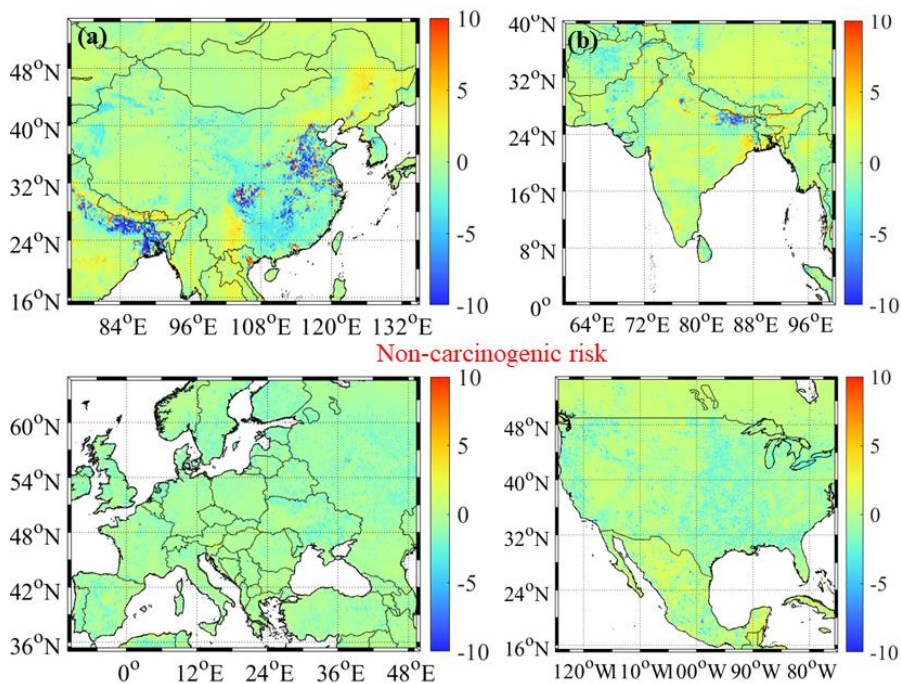




Table 1 The change ratio (%) of deweathered (P_{dew}) and detrended (P^*) benzene concentrations in major regions around the world.

Change ratio	China	India	Europe	United States
P_{dew} in 2020	-15.6	-23.6	-21.9	-16.2
P_{dew} in 2019	-2.31	-7.40	-8.04	-10.2
P^*	-13.3	-16.2	-13.9	-6.00

<https://doi.org/10.5194/egusphere-2022-1412>

Preprint. Discussion started: 2 January 2023

© Author(s) 2023. CC BY 4.0 License.

